Formation of a conducting $LaAlO_3/SrTiO_3$ interface studied by low-energy electron reflection during growth

A. J. H. van der Torren,[1] Z. Liao,[2] C. Xu,[3,*] N. Gauquelin,[4] C. Yin,[1] J. Aarts,[1,†] and S. J. van der Molen[1]
[1]*Huygens-Kamerlingh Onnes Laboratorium, Leiden University, Niels Bohrweg 2, 2300 RA Leiden, The Netherlands*
[2]*MESA+ Institute for Nanotechnology, University of Twente, P.O. Box 217, 7500 AE Enschede, The Netherlands*
[3]*Peter Grünberg Institute, Forachungscenter Jülich, 52425 Jülich, Germany*
[4]*EMAT, University Antwerp, Groenenborgerlaan 171, BE-2020 Antwerp, Belgium*
(Received 8 September 2017; published 6 December 2017)

The two-dimensional electron gas occurring between the band insulators $SrTiO_3$ and $LaAlO_3$ continues to attract considerable interest, due to the possibility of dynamic control over the carrier density and due to ensuing phenomena such as magnetism and superconductivity. The formation of this conducting interface is sensitive to the growth conditions, but despite numerous investigations there are still questions about the details of the physics involved. In particular, not much is known about the electronic structure of the growing $LaAlO_3$ layer at the growth temperature (around 800 °C) in oxygen (pressure around 5×10^{-5} mbar), since analysis techniques at these conditions are not readily available. We developed a pulsed laser deposition system inside a low-energy electron microscope in order to study this issue. The setup allows for layer-by-layer growth control and *in situ* measurements of the angle-dependent electron reflection intensity, which can be used as a fingerprint of the electronic structure of the surface layers *during* growth. By using different substrate terminations and growth conditions we observe two families of reflectivity maps, which we can connect either to samples with an AlO_2-rich surface and a conducting interface or to samples with a LaO-rich surface and an insulating interface. Our observations emphasize that substrate termination and stoichiometry determine the electronic structure of the growing layer, and thereby the conductance of the interface.

DOI: 10.1103/PhysRevMaterials.1.075001

I. INTRODUCTION

Transition-metal oxides, and in particular perovskites, form an important class of materials exhibiting a variety of physical phenomena such as superconductivity, magnetism, and ferroelectricity. Especially interesting for possible electronics applications is the occurrence of a two-dimensional electron gas between the two band insulators $LaAlO_3$ and $SrTiO_3$ [1]. The emergence of this conducting interface can at least partially be explained by the so-called polar catastrophe model. In this model an increasing electrical potential builds up when charged $(LaO)^+$ and $(AlO_2)^-$ layers are alternatively stacked on top of neutral layers of SrO and TiO_2. This potential is compensated by the transfer of half an electron charge from the surface to the interface. A relevant observation is that the electron gas only forms when the top $LaAlO_3$ layer is at least four unit cells thick [2]. At that thickness the potential buildup is apparently enough to transfer the charge to the interface. Furthermore, the electron gas only forms at the n-type interface (TiO_2/AlO_2) and not at the p-type interface (SrO/LaO) [1]. At the p-type interface a structural reconstruction is energetically favored over the electronic reconstruction [3].

Other observations, however, are at odds with a simple electronic reconstruction model. To name just two, electrical field buildup in the $LaAlO_3$ layer below the critical thickness is not observed [4,5], and samples grown in high oxygen partial pressure do not conduct [6,7]. Clearly, defects in the $LaAlO_3$ layer and in the TiO_2 termination layer also play an important role in the formation of the electron gas. Not surprisingly, therefore, it is very much the growth conditions which determine the conducting properties of the interface. In pulsed laser deposition (PLD), the exact plume shape and composition as well as the oxygen pressure are of great importance, influencing the cationic stoichiometry [8,9] of the $LaAlO_3$ film and the number of oxygen vacancies in the $SrTiO_3$ [10]. In particular, a La/Al ratio exceeding 0.97 [8] was shown to fully suppress the conductivity. Similarly, high-pressure oxygen sputtering yielded a La/Al ratio well above 1 and nonconducting interfaces [11]. Also the occurrence of magnetism [10,12–14] and superconductivity [15–17] was shown to be sensitive to the oxygen pressure during growth.

Whereas differences in growth conditions are therefore known to lead to conducting or insulating samples as measured afterwards, little is known about how the electronic properties of the material develop during growth, mainly because the high temperatures and high oxygen pressure required during growth limit the abilities for *in situ* analysis. For this reason we recently developed an *in situ* pulsed laser deposition system inside a low-energy electron microscope. This allows us to follow the growth by monitoring oscillations in the width and intensity of the specular beam [18]. At the same time, it allows measurements of the angle-dependent electron reflectivity of the surface with sub-unit-cell precision, which yields information on the unoccupied part of the band structure [19,20]. Here we show the results of the growth of $LaAlO_3$ on $SrTiO_3$ under different circumstances. We find clear differences in the development of the reflectivity maps when growing samples with conducting or with insulating interfaces,

*Present address: Institut für Solarenergieforschung GmbH Hameln/Emmerthal, Am Ohrberg 1, 31860 Emmerthal, Germany.
†aarts@physics.leidenuniv.nl

and relate that to the surface termination and stoichiometry of the growing film.

II. EXPERIMENTAL SETUP AND SAMPLE PREPARATION

The $LaAlO_3/SrTiO_3$ interfaces are grown and studied in an aberration corrected low-energy electron microscope (LEEM) at Leiden university, called ESCHER [21–24]. The LEEM technique has been used before to study $SrTiO_3$ [25] and $LaAlO_3$ [26] separately. We now also developed a PLD system inside the system to allow for analysis during growth, which was already used to study the growth of $SrTiO_3$ on $SrTiO_3$ [18]. In order to study growth, pulsed deposition is performed alternatingly with LEEM imaging. In more detail, between every few laser/deposition pulses, the LEEM is turned on (meaning the high voltage between objective lens and sample, required for the low-energy electrons, is switched on) and diffraction images are obtained. From the diffraction images the intensity and shape of the specular diffraction spot are determined to monitor the growth. After this measurement the high voltage is turned off and deposition can continue. For growth monitoring we obtain the full width at half maximum (FWHM) and the peak intensity of the specular spot. In a layer-by-layer growth mode, both the FWHM and the intensity oscillate, out of phase with one another, and allow precise control over the deposition. To obtain a fingerprint of the unoccupied band structure, angle-resolved reflected electron spectroscopy (ARRES) is also performed [19,20]. In this technique the electron reflection is measured depending on energy and on the in-plane wave vector, which is controlled by the angle of incidence of the electron beam. ARRES utilizes the fact that the electron reflectivity strongly depends on the electron landing energy E_0 and the in-plane momentum $k_\parallel$. In particular the electron reflection is low if the material has a band at the specific $(E_0, k_\parallel)$ of the electron so that it can couple into the band. In contrast, when $(E_0, k_\parallel)$ of the electron coincide with a band gap the electron reflectivity is high. Hence the "reflected-electron" or ARRES map shows a fingerprint of the unoccupied band structure. For the ARRES measurements we obtain the total (integrated) spot intensity which is independent of the surface roughness, i.e., the total intensity stays constant when the surface roughens since the spot broadening lowers the maximum.

As substrates, $SrTiO_3$ (100) single crystals from CrysTec GmbH are used which were TiO_2 terminated by a buffered HF etch [27] and annealing in oxygen at 950 °C for 1 h. The SrO-terminated substrate was prepared in a different PLD system by growing a double SrO layer on a TiO_2-terminated substrate. For the PLD targets, single crystals $LaAlO_3$ (100) from Crystal GmbH were used. PLD is performed using an aperture in the laser beam path, which is imaged on the target by a lens. The PLD growth is performed at a pressure of 5.5×10^{-5}-mbar oxygen and if not otherwise stated at a 2-J/cm^2 laser fluence with 1-Hz repetition rate. Depending on deposition speed, the deposition is briefly intermitted each 5 to 50 pulses to perform imaging and spectroscopy. This results in around ten measurements per unit cell grown. Samples are grown at temperatures between 800 and 860 °C as measured with a pyrometer (emissivity 0.8). Temperature-dependent resistance measurements were performed in a physical properties measurement system (Quantum Design) in a van der Pauw configuration. In order to facilitate the discussion, samples with a conducting interface will henceforth be designated with the suffix "C" and insulating samples will be labeled "I." The composition across the interface was measured by scanning transmission electron microscopy (STEM) in electron energy-loss (EELS) mode on a Titan microscope operated at 300 kV. Samples were prepared by focused ion beam (milling) as described elsewhere [28]. The profiles shown below [Fig. 5(b)] result from the average of five different measurements. The integrated intensity of the Sr L edge, Ti L edge, La M edge, and Al K edge was normalized by dividing by the maximum. A slight cation deficiency was ignored due to the limited precision of EELS quantification (as discussed in Ref. [29]).

III. RESULTS

Three $LaAlO_3/SrTiO_3$ heterostructures were grown under two different growth conditions and on two kinds of substrates. The first sample (S1-C) was grown with an optimal fluence of 2 J/cm^2 on a TiO_2-terminated $SrTiO_3$ substrate, and the second sample (S2-I) was grown with a much lower fluence *by changing the lens position, which increases the spot size and lowers the fluence* on the same TiO_2-terminated substrate. *Note that this in general will also change the plume characteristics*. The third sample (S3-I) was grown with the optimal fluence of 2 J/cm^2 on the SrO-terminated $SrTiO_3$ substrate. For layer-by-layer growth control we took low-energy electron-diffraction images as shown in Fig. 1(a) for bare $SrTiO_3$. The starting surface shows clear diffraction spots and a 2×1 reconstruction, in line with earlier observations [25]. From the diffraction images, the peak intensity and FWHM of the specular spot were recorded and are shown in Figs. 1(b), 1(c) and 1(d) in red and blue, respectively, for samples S1-C, S2-I, and S3-I.

Clear oscillations can be observed in both FWHM and peak intensity, which are out of phase with one another. The landing energy of the electrons (17 eV) has been optimized for maximal contrast in the oscillations. This energy is close to the out-of-phase condition where the electrons destructively interfere at the step edges on the surface. At the flat surface the coherent areas are large, resulting in sharp diffraction spots with small FWHM. When the surface roughens during growth the coherent areas become small due to the large amounts of newly grown islands, which results in low peak intensity and high FWHM. As a guide to the eye, dotted lines are plotted to indicate integer number of unit cells grown. A total of eight unit cells were grown on S1-C and S2-I, and five unit cells were grown on S3-I. Many more pulses were needed for sample S2-I [Fig. 1(c)] than sample S1-C and S3-I [Figs. 1(b) and 1(d)]. From this we can conclude that the growth speed is highly reduced for the out-of-focus laser beam, as expected. For sample S1-C [Fig. 1(b)] the peak intensity strongly decreases at the start to oscillate around a constant background for the remainder of the time. Sample S2-I shows the same decrease of background intensity up to two unit cells, but then comes back to the starting value between three and five unit cells. Sample S3-I does not show the decrease at the start and keeps oscillating around a constant value. This change in background intensity is related to the electronic structure of the surface layer as will become clear below. First we characterize the

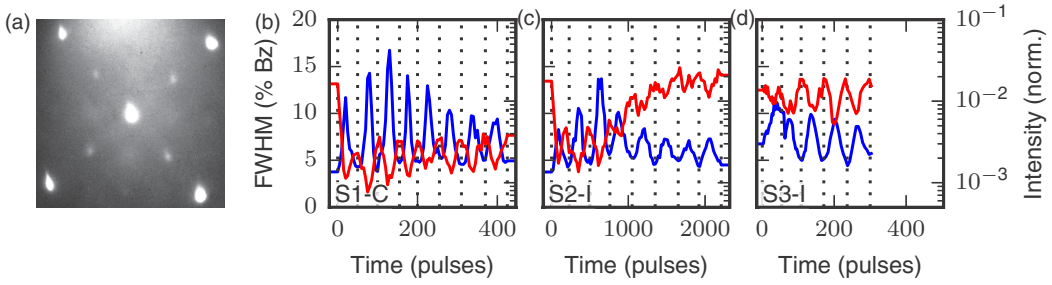

FIG. 1. (a) Diffraction pattern on bare $SrTiO_3$ at a growth temperature of 820 °C taken at 17 eV. (b) FWHM (blue) and maximum intensity (red) of the specular diffraction spot for a conducting sample S1-C. (c) Same for the insulating sample S2-I. (d) Same for the insulating sample S3-I. All data have been taken at 17-eV landing energy. The FWHM is given in percentage of the Brillouin zone, which is equal to the percentage of the distance from specular to first-order spots. The intensity has been normalized at the mirror mode (zero landing energy) intensity.

electrical properties of these samples. For this, the temperature dependence of the sheet resistance was measured and is shown in Fig. 2(a) for sample S1-C (blue), sample S2-I (green), and sample S3-I (cyan). Sample S1-C shows conducting behavior while sample S2-I and sample S3-I are insulating.

To fingerprint the difference between conducting and insulating samples at the growth temperature, we use ARRES [19] as shown in Figs. 2(b)–2(f). ARRES maps of sample S1-C, S2-I, and S3-I are shown in Figs. 2(b), 2(d) and 2(e), respectively. These maps were measured directly after growth, at the growth temperature. The differences between the conducting and the nonconducting samples are large. The conducting sample S1-C [Fig. 2(b)] shows a band (minimum in intensity) around 14 eV at the Γ point and a V-shaped band at the top of the figure above 20 eV, while the insulating samples S2-I and S3-I [Figs. 2(d) and 2(e)] show a maximum (i.e., a band gap) between 14 and 22 eV around the Γ point.

In order to see whether this correlation is general, we measured two samples grown in other systems in ways which are known from literature to produce conducting and nonconducting samples. Sample S4-C was grown in a conventional PLD system with the possibility to grow under higher oxygen pressures which is known to result in conducting samples. Sample S5-I was grown by on-axis sputter deposition, known to result in insulating samples [11]. ARRES maps are shown in Figs. 2(c) and 2(f) for S4-C and S5-I, respectively. Their (non-)conductance is confirmed by electrical measurements [Fig. 2(a)]. During the ARRES measurements, both samples were kept at a high temperature in an oxygen pressure of 5×10^{-5} mbar to remove any contaminants and prevent the surface from charging. Exact growth and measurement conditions can be found in the Appendix. Comparing S1-C and S4-C we conclude the ARRES maps are similar and not sensitive to *ex situ* transfer. The insulating samples S2-I, S3-I, and S5-I in the bottom row of Fig. 2 are also similar, which leads us to conclude that the differences are intrinsic.

Next we consider the change of the reflectivity with thickness. Figure 3 shows ARRES maps at the growth temperature for every second unit cell grown. Conducting sample S1-C is shown at the top [Figs. 3(a)–3(e)] and insulating sample S2-I is shown at the bottom [Figs. 3(g)–3(k)]. Both samples start with a TiO_2-terminated $SrTiO_3$ surface (a, g), showing the same map only slightly different in brightness. The maps show a strong change as soon as two unit cells of $LaAlO_3$ are

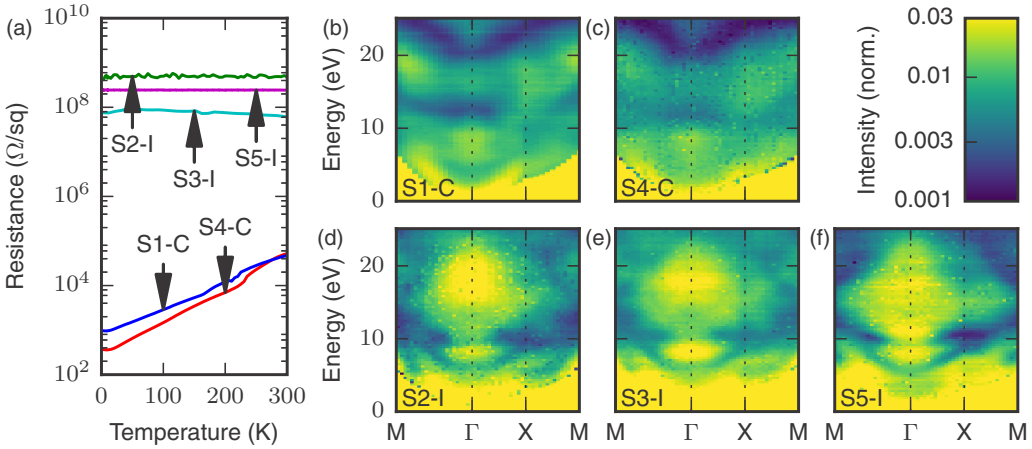

FIG. 2. (a) Sheet resistance vs temperature for five different samples. (b–f) ARRES measurements for conducting (S1-C, S4-C) and nonconducting (S2-I, S3-I, S5-I) samples. Sample S1-C (b, blue), eight unit cells of $LaAlO_3$ grown in the LEEM; sample S4-C (c, red), four unit cells of $LaAlO_3$ grown in a conventional PLD setup; sample S2-I (d, green), eight unit cells of $LaAlO_3$ grown with an out-of-focus PLD laser; sample S3-I (e, cyan), five unit cells of $LaAlO_3$ grown on SrO-terminated $SrTiO_3$; and sample S5-I (f, magenta), 5-nm $LaAlO_3$ grown with sputter deposition.

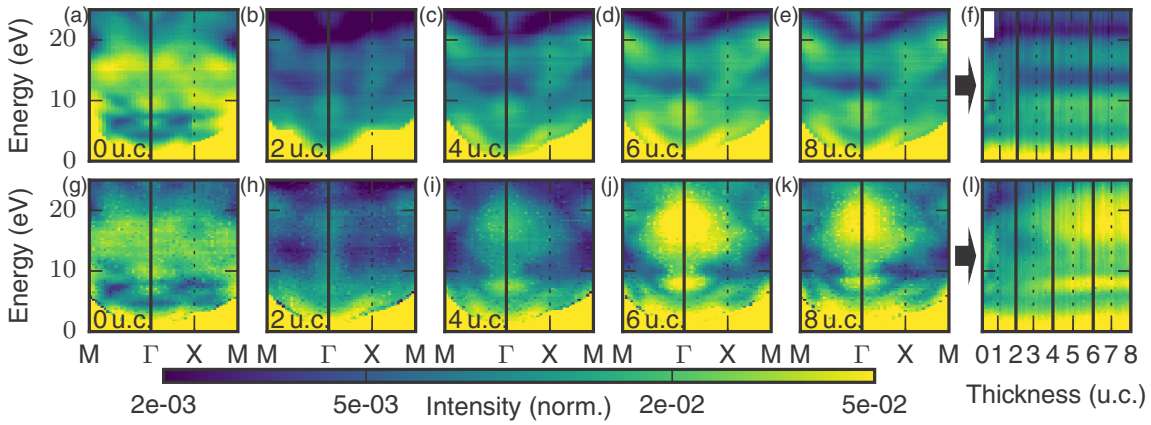

FIG. 3. Conducting sample S1-C (top, a–f) and nonconducting sample S2-I (bottom, g–l). From left to right: ARRES maps for zero (a, g), two (b, h), four (c, i), six (d, j), and eight (e, k) unit cells, respectively, and an IV-curve vs thickness map (f, l). The black vertical lines at the Γ point in the ARRES maps correspond with the black vertical lines in the IV-curve map including left and right edges. All images have the same color intensity.

grown (b, h). However, the maps of the conducting sample S1-C (top, b) and insulating sample S2-I (bottom, h) still show many similarities. This changes at four unit cells of $LaAlO_3$. While for the conducting sample S1-C [Fig. 3(c)] the band around Γ at 14 eV becomes a little bit more pronounced, the nonconducting sample S2-I [Fig. 3(i)] strongly changes and develops a pronounced band gap around the Γ point for energies between 14 and 22 eV, observed as a high-intensity area. Adding more $LaAlO_3$ up to six [Figs. 3(d) and 3(j)] and eight [Figs. 3(e) and 3(k)] unit cells only leads to little changes, both for the conducting and the nonconducting samples.

To probe the changes during growth in more detail we focus on the electron reflectivity at the Γ point ($k_{\parallel} = 0$). This is nothing else than a LEEM (or LEED) IV curve, which is the intensity variation of a diffracted beam, in this case the specular beam, as a function of electron energy. Such curves are indicated with a vertical black line in the ARRES maps in Fig. 3. These curves were taken during growth at regular intervals of eight to ten times per unit cell. Results are shown in Figs. 3(f) and 3(l) [sample S1-C top, f and sample S2-I bottom, l]. They show the gradual change from the $SrTiO_3$ fingerprint to the final IV curve of the $SrTiO_3/LaAlO_3$ heterostructure. The five solid black vertical lines between zero and eight unit cells correspond to the lines at the Γ point in the five ARRES maps on the left side of Fig. 3. The IV-curve map Fig. 3(f) shows that the band at 14 eV in sample S1-C appears just after two unit cells have been grown. The band around 21 eV has already appeared at this thickness. The nonconducting sample S2-I [Fig. 3(l)] shows both bands around two unit cells, but they vanish between three and four unit cells when the band gap appears between 14 and 22 eV. The band gap at 8 eV also clearly appears at this thickness.

Still for samples S1-C and S2-I a zoomed-in part of the IV-curve maps for zero to five unit cells is shown in Figs. 4(a) and 4(b) together with an IV-curve map of sample S3-I with $LaAlO_3$ on SrO-terminated $SrTiO_3$ [Fig. 4(c)], the substrate prepared in a different PLD system. For comparison, the IV curves after deposition of zero, two, and five unit cells of $LaAlO_3$ are plotted in Figs. 4(d)– 4(f). Here the IV curves from sample S1-C are plotted in blue, those from sample S2-I are plotted in green, and those from sample S3-I are plotted in red. These plots clearly show two distinct IV curves at zero unit cells and two distinct IV curves after deposition of five unit cells of $LaAlO_3$. The starting IV curves at zero unit cells correspond with the TiO_2-terminated (blue, green) and SrO-terminated (red) $SrTiO_3$ while in the IV curves after deposition we distinguish the conducting (blue) and nonconducting (green, red) samples. The evolution of the IV curves during growth is different for the two insulating samples. This is very clear around two unit cells where sample S2-I (green) is still close to sample S1-C (blue) and not to sample S3-I (red), which is already close to the insulating final IV fingerprint found on the nonconducting samples. As a matter of fact, the IV curves for S3-I hardly change during growth on the SrO-terminated surface.

With these results, we can return to Fig. 1, where for sample S1-C the intensity strongly decreased at the start and continued to oscillate around a low value; for sample S2-I the intensity decreased at the start, but recovered between three and five unit cells, and for sample S3-I the intensity oscillated around the starting value and did not decrease at all. The energy of 17 eV where the data of Fig. 1 were taken is indicated with a horizontal dotted line in the IV-curve maps, Figs. 4(a)– 4(c). Note that in Fig. 1 the maximum of the specular diffraction spot is plotted, which is sensitive to spot broadening due to surface roughening. This results in growth oscillations superimposed on the electron reflectivity signal. On the other hand, for Fig. 4 the intensity of the total specular spot is integrated, resulting in an intensity independent of spot shape (i.e., surface roughness) and only depending on the electron reflectivity. Combining Figs. 1 and 4 we can now conclude that the increasing background signal between three and four unit cells in Fig. 1(c) is caused by the appearance of the band gap (enhanced surface reflectivity) shown in Fig. 4(b).

One question with respect to the out-of-focus grown sample is whether the epitaxy is impaired by the ill-defined fluence. For that we performed STEM experiments with high-angle annular dark-field imaging (HAADF). Samples S6-I, S7-C, and S8-I were prepared in the same conditions as samples

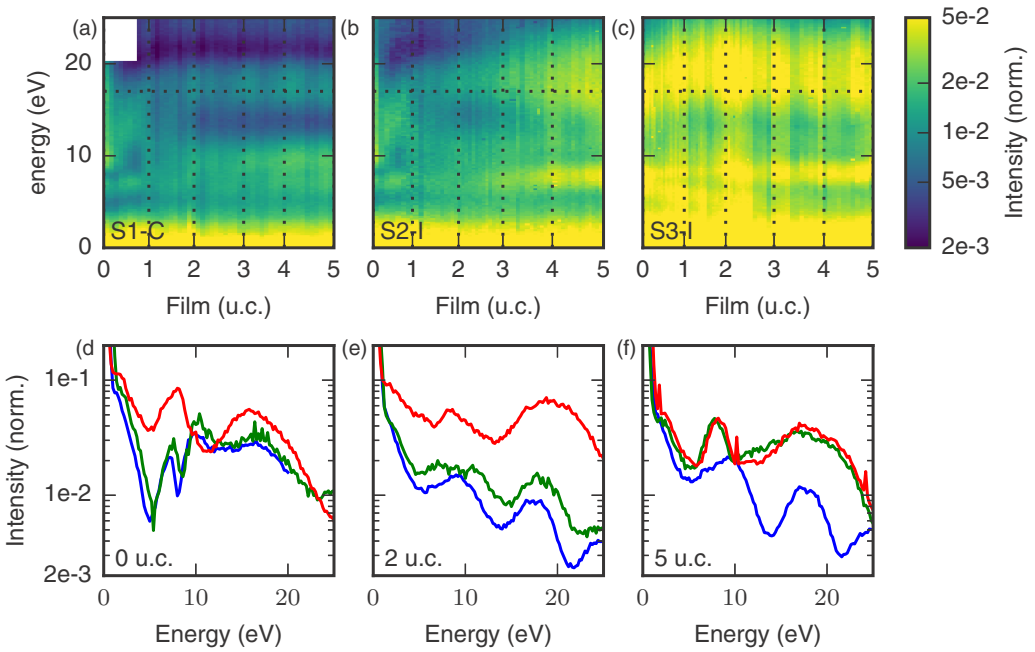

FIG. 4. IV-curve vs thickness maps for sample S1-C (a), sample S2-I (b), and sample S3-I (c). (d, e, f) IV curves after deposition of zero, two, and five unit cells of $LaAlO_3$, respectively, for sample S1-C (blue), sample S2-I (green), and sample S3-I (red). Horizontal dotted lines in panels (a)–(c) indicate the energy where Fig. 1 was measured. IV curves are obtained by the integrated intensity of the specular diffraction spot, filtering out any influence of the surface roughness.

S2-I, S4-C, and S3-I. For the sake of avoiding any surface influence on the compositional analysis, thick films of 20UC were grown. Figure 5(a) presents a typical STEM-HAADF of the $LaAlO_3$ film on the $SrTiO_3$ substrate. Besides a slight misorientation of the nonconducting films with respect to the substrate, good quality epitaxial growth was observed for all samples. Figure 5(b) shows the La and Ti occupancies normalized to the total A- and B-site occupancy for samples S6-I (defocused), S7-C, and S8-I (SrO terminated) in blue triangles, red squares, and black circles, respectively. The A site is represented by filled symbols, and the B site is represented by empty symbols. A similar extent of Ti diffusion into the $LaAlO_3$ (four to five unit cells) can be observed for all samples, including the out-of-focus sample S6-I. As expected, the concentration of Ti in those first unit cells of the LaO film is higher, reflecting the Al deficiency of the growing film. On the other hand, the La/Sr intermixing is similar for samples S6-I and S7-C but Sr diffuses much further for sample S8-I (SrO terminated), leading to a relatively lower La content. We can therefore conclude that the A-site interdiffusion is controlled by the substrate termination and not influenced by the out-of-focus condition.

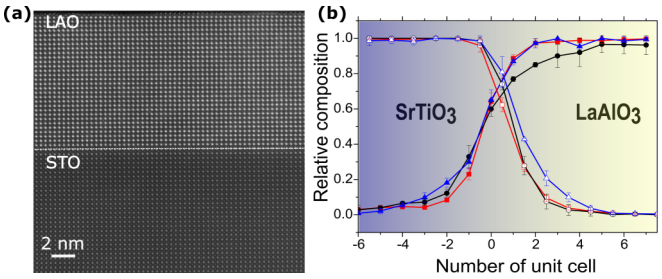

FIG. 5. (a) STEM-HAADF image in the [100] orientation of sample S6-I grown under the same conditions as S2-I but with 20 unit cells of $LaAlO_3$. Images for samples S7-C and S8-I show the same epitaxial quality. (b) Normalized La (filled symbols) and Ti (open symbols) occupancies for S6-I (blue triangles); S7-C (red squares) and S8-I (black circles) are obtained from EELS measurements.

IV. DISCUSSION

As mentioned in the introduction, the model of electronic reconstruction of a basically perfect interface is not enough to explain the occurrence of conductance. Questions then exist about the relative importance of the role of intermixing, oxygen vacancies, strain gradients with their ensuing buckling of the oxygen octahedra at the interface, and the stoichiometry of the $LaAlO_3$ layer. The discussion on the La/Al stoichiometry has started relatively recently. It has been found that the $LaAlO_3$ film has to be Al rich for conductance to appear [8,9], and also that the $LaAlO_3$ stoichiometry is strongly dependent on the PLD parameters. In Ref. [30] it was shown that decreasing the fluence by 25% from the value which produces a La/Al ratio of 1 leads to an increase of that ratio to 1.05, which is enough to increase the typical resistivity by four orders of magnitude. We will now argue that our electron reflectivity experiments precisely address the issues of stoichiometry and defects, which are crucial for the occurrence of interface conductivity. Our observations are that (i) the difference between C and I samples is already apparent during growth and at the growth temperature and (ii) the differences between C and I samples are significant on the eV scale. The conclusion we draw from this is that the (electronic) structure of the $LaAlO_3$ surface layer, which is what our experiment is most sensitive to, is different for C samples and for I samples. The sensitivity of the

electron reflectivity to the surface layer can be demonstrated from the strong change in IV curve seen in Fig. 4(d) between TiO_2-terminated and SrO-terminated $SrTiO_3$. We note that the sensitivity depends on the penetration depth, which is energy dependent. Unfortunately, calculations of the electron reflectivity or the empty band structure of different possible surfaces do not yet exist in the measured energy range. We can, however, sketch a scenario which can be considered for such calculations.

We start with noting that the $LaAlO_3$ grown on TiO_2-terminated $SrTiO_3$ should be AlO_2 terminated, while the $LaAlO_3$ grown on SrO-terminated $SrTiO_3$ should be LaO terminated. We surmise that this difference in termination causes the strong difference between the conducting sample S1-C and the nonconducting sample S3-I. Consider now sample S2-I, which shows an IV curve comparable to sample S1-C (AlO_2 terminated) for two unit cells [Fig. 4(e)] but changes to the signature of sample S3-I (LaO terminated) for five unit cells [Fig. 4(f)]. In contrast to the other samples, sample S2-I was grown with an out-of-focus laser. As mentioned above, a change in fluence means a change in stoichiometry. The sheet resistance value of the order of 100 MΩ/sq can be compared to the value of 10 MΩ/sq we found for sputtered films with an excess of 7% La [11], and with a value of 0.5 MΩ/sq reported for films with 5% excess La [9]. From this we would tentatively estimate the La excess in sample S2-I to be in the range 7 to 10%. The crystal structure easily accommodates defects, and such an excess would not readily show up in the TEM image. Next, we know that Al-rich $LaAlO_3$ results in a conducting interface and La-rich $LaAlO_3$ results in an insulating interface. From this we infer that sample S2-I, grown with an out-of-focus laser, is La rich. In growing S2-I, growth on TiO_2-terminated $SrTiO_3$ first results in a AlO_2 termination, as seen after growth of two unit cells. Growing further, the La excess slowly builds up, changing the surface to LaO rich. We note that the Ti intermixing into the $LaAlO_3$ found for sample S2-I could compensate the Al deficits in the first unit cells, suppressing the effects of the La excess in those cells. Here we should remark that density functional theory calculations in Ref. [31] showed that surfaces are not AlO_2 or LaO terminated, but rather $Al_{3/2}O_2$ and $La_{5/6}O$ are the stable surface terminations. This implies that the AlO_2 surfaces mentioned above are actually $Al_{3/2}O_2$ and the LaO surface is $La_{5/6}O$, which does not conflict with our results. On the contrary, the fact that less La is required for the $La_{5/6}O$ and more Al is required for the $Al_{3/2}O_2$ surface could stimulate the transition from a $Al_{3/2}O_2$ to a $La_{5/6}O$ surface for our La-rich sample S2-I. All in all, we argue that the strong change in electron reflectivity, which is correlated to the unoccupied band structure, depends on the surface termination. From the importance of the surface for the interface conductivity as described in literature [32–34] and our findings we deduce that the excess La in the surface layer could be an essential ingredient in suppressing the electron transfer to the interface. More research has to be done to investigate the exact mechanism, *which clearly goes well beyond the simple polar catastrophe model*. Finally, we note that our La-rich and Al-rich surface signatures do not correspond with the IV curves measured on bulk mixed ordered terminated $LaAlO_3$ as reported before [26]. This can, however, be explained by the surface reconstructions found on the bulk $LaAlO_3$ and the difference between bulk and strained thin films.

V. SUMMARY

We have shown results of electron reflectivity experiments (ARRES) on conducting and insulating $LaAlO_3/SrTiO_3$ heterostructures during growth, at the growth temperature with sub-unit-cell precision. We find distinct signatures for the conducting and nonconducting samples independent of their growth conditions. In other words, the electron reflectivity (ARRES) can predict *during growth* whether a sample will show conductivity.

We find that the two families of reflectivity curves (maps) can be assigned to what we argue are different surface terminations, either AlO_2 or LaO rich. For samples with Al-rich $LaAlO_3$ the surface termination is directly coupled to the termination of the $SrTiO_3$. A SrO termination results in a LaO-rich surface, while a TiO_2 termination results in an AlO_2-rich surface. For the growth of La-rich $LaAlO_3$, which we believe we achieve by out-of-focus laser growth, we find the surface termination slowly changes from AlO_2 rich to LaO rich during growth. From the importance of the surface for the interface conductivity as described in literature [32–34], we infer that it could be this change in surface termination that is essential in suppressing the interface conductivity for the La-rich growth. At the same time, it once more emphasizes that the termination which promotes interface conductivity makes that conductivity sensitive to surface charges.

ACKNOWLEDGMENTS

We acknowledge Ruud Tromp, Daniel Geelen, Johannes Jobst, Regina Dittmann, Gert Jan Koster, Guus Rijnders, and Jo Verbeek for discussions and advice and Ruud van Egmond and Marcel Hesselberth for technical assistance. This work was supported by the Netherlands Organization for Scientific Research (NWO) by means of an NWO Groot grant and by the Leiden-Delft Consortium NanoFront. This work is part of the research programs NWOnano and DESCO, which are financed by NWO. N.G. acknowledges funding through the GOA project Solarpaint of the University of Antwerp and from FWO Project No. G.0044.13N (charge ordering). The microscope used in this work was partly funded by the Hercules Fund from the Flemish Government. We would also like to acknowledge networking support by the COST Action MP 1308 (COST TO-BE).

TABLE I. PLD and sputter growth conditions for samples analyzed in LEEM as well as the temperature at which the ARRES maps were taken.

Sample no.	Fluence (J/cm^2)	Growth (°C)	Termination	Pressure (mbar)	ARRES (°C)
S1-C	2	780	TiO_2	5×10^{-5}	795
S4-C	1	720	TiO_2	1×10^{-4}	630
S2-I	Defocus	770	TiO_2	5×10^{-5}	770
S3-I	2	700	SrO	5×10^{-5}	600
S5-I		830	TiO_2	3×10^{0}	560

APPENDIX

Five samples have been grown for LEEM analysis. The growth parameters of these films for PLD (S1-4) and sputtering (S5) are shown in Table I together with the temperature at which the ARRES maps are measured.

[1] A. Ohtomo and H. Y. Hwang, Nature (London) **427**, 423 (2004).

[2] S. Thiel, G. Hammerl, A. Schmehl, C. W. Schneider, and J. Mannhart, Science **313**, 1942 (2006).

[3] L. Zhang, X.- Feng Zhou, H.-T. Wang, J.-J. Xu, J. Li, E. G. Wang, and Su-Hai Wei, Phys. Rev. B **82**, 125412 (2010).

[4] Y. Segal, J. H. Ngai, J. W. Reiner, F. J. Walker, and C. H. Ahn, Phys. Rev. B **80**, 241107 (2009).

[5] E. Slooten, Z. Zhong, H. J. A. Molegraaf, P. D. Eerkes, S. de Jong, F. Massee, E. van Heumen, M. K. Kruize, S. Wenderich, J. E. Kleibeuker, M. Gorgoi, H. Hilgenkamp, A. Brinkman, M. Huijben, G. Rijnders, D. H. A. Blank, G. Koster, P. J. Kelly, and M. S. Golden, Phys. Rev. B **87**, 085128 (2013).

[6] G. Herranz, M. Basletić, M. Bibes, C. Carrétéro, E. Tafra, E. Jacquet, K. Bouzehouane, C. Deranlot, A. Hamzić, J.-M. Broto, A. Barthélémy, and A. Fert, Phys. Rev. Lett. **98**, 216803 (2007).

[7] A. Kalabukhov, Yu. A. Boikov, I. T. Serenkov, V. I. Sakharov, J. Börjesson, N. Ljustina, E. Olsson, D. Winkler, and T. Claeson, Europhys. Lett. **93**, 37001 (2011).

[8] M. P. Warusawithana, C. Richter, J. A. Mundy, P. Roy, J. Ludwig, S. Paetel, T. Heeg, A. A. Pawlicki, L. F. Kourkoutis, M. Zheng, M. Lee, B. Mulcahy, W. Zander, Y. Zhu, J. Schubert, J. N. Eckstein, D. A. Muller, C. S. Hellberg, J. Mannhart, and D. G. Schlom, Nat. Commun. **4**, 2351 (2013).

[9] E. Breckenfeld, N. Bronn, J. Karthik, A. R. Damodaran, S. Lee, N. Mason, and L. W. Martin, Phys. Rev. Lett. **110**, 196804 (2013).

[10] A. Brinkman, M. Huijben, M. van Zalk, J. Huijben, U. Zeitler, J. C. Maan, W. G. van der Wiel, G. Rijnders, D. H. A. Blank, and H. Hilgenkamp, Nat. Mat. **6**, 493 (2007).

[11] I. M. Dildar, D. B. Boltje, M. H. S. Hesselberth, J. Aarts, Q. Xu, H. W. Zandbergen, and S. Harkema, Appl. Phys. Lett. **102**, 121601 (2013).

[12] Ariando X. Wang, G. Baskaran, Z. Q. Liu, J. Huijben, J. B. Yi, A. Annadi, A. Roy Barman, A. Rusydi, S. Dhar, Y. P. Feng, J. Ding, H. Hilgenkamp, and T. Venkatesan, Nat. Commun. **2**, 188 (2011).

[13] D. A. Dikin, M. Mehta, C. W. Bark, C. M. Folkman, C. B. Eom, and V. Chandrasekhar, Phys. Rev. Lett. **107**, 056802 (2011).

[14] J. A. Bert, B. Kalisky, C. Bell, M. Kim, Y. Hikita, H. Y. Hwang, and K. A. Moler, Nat. Phys. **7**, 767 (2011).

[15] N. Reyren, S. Thiel, A. D. Caviglia, L. F. Kourkoutis, G. Hammerl, C. Richter, C. W. Schneider, T. Kopp, A.-S. Rütschi, D. Jaccard, M. Gabay, D. A. Muller, J.-M. Triscone, and J. Mannhart, Science **317**, 1196 (2007).

[16] A. Joshua, S. Pecker, J. Ruhman, E. Altman, and S. Ilani, Nat. Commun. **3**, 1129 (2012).

[17] A. D. Caviglia, S. Gariglio, N. Reyren, D. Jaccard, T. Schneider, M. Gabay, S. Thiel, G. Hammerl, J. Mannhart, and J.-M. Triscone, Nature (London) **456**, 624 (2008).

[18] A. J. H. van der Torren, S. J. van der Molen, and J. Aarts, Nanotechnology **27**, 495702 (2016).

[19] J. Jobst, J. Kautz, D. Geelen, R. M. Tromp, and S. J. van der Molen, Nat. Commun. **6**, 8926 (2015).

[20] J. Jobst, A. J. H. van der Torren, E. E. Krasovskii, J. Balgley, C. R. Dean, R. M. Tromp, and S. J. van der Molen, Nat. Commun. **7**, 13621 (2016).

[21] R. M. Tromp, J. B. Hannon, A. W. Ellis, W. Wan, A. Berghaus, and O. Schaff, Ultramicroscopy **110**, 852 (2010).

[22] S. M. Schramm, J. Kautz, A. Berghaus, O. Schaff, R. M. Tromp, and S. J. van der Molen, IBM J. Res. Dev. **55**, 1 (2011).

[23] S. M. Schramm, A. B. Pang, M. S. Altman, and R. M. Tromp, Ultramicroscopy **115**, 88 (2012).

[24] R. M. Tromp, J. B. Hannon, W. Wan, A. Berghaus, and O. Schaff, Ultramicroscopy **127**, 25 (2013).

[25] M. B. S. Hesselberth, S. J. van der Molen, and J. Aarts, Appl. Phys. Lett. **104**, 051609 (2014).

[26] A. J. H. van der Torren, S. J. van der Molen, and J. Aarts, Phys. Rev. B **91**, 245426 (2015).

[27] M. Kawasaki, K. Takahashi, T. Maeda, R. Tsuchiya, M. Shinohara, O. Ishiyama, T. Yonezawa, M. Yoshimoto, and H. Koinuma, Science **266**, 1540 (1994).

[28] Y. Z. Chen, F. Trier, T. Wijnands, R. J. Green, N. Gauquelin, R. Egoavil, D. V. Christensen, G. Koster, M. Huijben, N. Bovet, S. Macke, F. He, R. Sutarto, N. H. Andersen, J. A. Sulpizio, M. Honig, G. We. D. K. Prawiroatmodjo, T. S. Jespersen, S. Linderoth, S. Ilani, J. Verbeeck, G. Van Tendeloo, G. Rijnders, G. A. Sawatzky, and N. Pryds, Nat. Mat. **14**, 801 (2015).

[29] N. Gauquelin, E. Benckiser, M. K. Kinyanjui, M. Wu, Y. Lu, G. Christiani, G. Logvenov, H.-U. Habermeier, U. Kaiser, B. Keimer, and G. A. Botton, Phys. Rev. B **90**, 195140 (2014).

[30] E. Breckenfeld, R. Wilson, and L. W. Martin, Appl. Phys. Lett. **103**, 082901 (2013).

[31] C. Weiland, G. E. Sterbinsky, A. K. Rumaiz, C. S. Hellberg, J. C. Woicik, S. Zhu, and D. G. Schlom, Phys. Rev. B **91**, 165103 (2015).

[32] Y. Xie, C. Bell, T. Yajima, Y. Hikita, and H. Y. Hwang, Nano Lett. **10**, 2588 (2010).

[33] R. Pentcheva, R. Arras, K. Otte, V. G. Ruiz, and W. E. Pickett, Phil. Trans. R. Soc. A **370**, 4904 (2012).

[34] K. A. Brown, Shu He, D. J. Eichelsdörfer, Mengchen Huang, I. Levy, Hyungwoo Lee, Sangwoo Ryu, P. Irvin, J. Mendez-Arroyo, C.-B. Eom, C. A. Mirkin, and J. Levy, Nat. Commun. **7**, 10681 (2016).